



HAL
open science

Magma reservoir growth and ground deformation preceding the 79 CE Plinian eruption of Vesuvius

Domenico M Doronzo, Elisa Trasatti, Ilenia Arienzo, H el ene Balcone-Boissard, Diana Barra, Giuseppe Aiello, Vincenzo Amato, Mauro Di Vito

► **To cite this version:**

Domenico M Doronzo, Elisa Trasatti, Ilenia Arienzo, H el ene Balcone-Boissard, Diana Barra, et al.. Magma reservoir growth and ground deformation preceding the 79 CE Plinian eruption of Vesuvius. Communications Earth & Environment, 2023, 4 (1), pp.211. 10.1038/s43247-023-00880-9 . hal-04128823

HAL Id: hal-04128823



<https://hal.science/hal-04128823>

Submitted on 14 Jun 2023

HAL is a multi-disciplinary open access archive for the deposit and dissemination of scientific research documents, whether they are published or not. The documents may come from teaching and research institutions in France or abroad, or from public or private research centers.

L'archive ouverte pluridisciplinaire **HAL**, est destin ee au d ep ot et  a la diffusion de documents scientifiques de niveau recherche, publi es ou non,  emanant des  tablissements d'enseignement et de recherche fran ais ou  trangers, des laboratoires publics ou priv es.

Magma reservoir growth and ground deformation preceding the 79 CE Plinian eruption of Vesuvius

Domenico M. Doronzo¹[✉], Elisa Trasatti², Ilenia Arienzo¹, H el ene Balcone-Boissard³, Diana Barra⁴, Giuseppe Aiello⁴, Vincenzo Amato⁵ & Mauro A. Di Vito¹

The 79 CE eruption of Vesuvius is the first documented Plinian eruption, also famous for the archaeological ruins of Pompeii and Herculaneum. Although much is known regarding the eruption dynamics and magma reservoir, little is known about the reservoir shape and growth, and related ground deformation. Numerical modelling by Finite Element Method was carried out, aimed at simulating the reservoir growth and ground deformation with respect to the reservoir shape (prolate, spherical, oblate) and magma overpressure. The modelling was tuned with volcanological, petrological and paleoenvironmental ground deformation constraints. Results indicate that the highest magma overpressure is achieved considering a prolate reservoir, making it as the most likely shape that led to eruption. Similar deformations but lower overpressures are obtained considering spherical and oblate reservoirs. These results demonstrate that ground deformation may not be indicative of eruption probability, style/size, and this has direct implications on surveillance at active explosive volcanoes.

¹Istituto Nazionale di Geofisica e Vulcanologia, Osservatorio Vesuviano, Naples, Italy. ²Istituto Nazionale di Geofisica e Vulcanologia, Osservatorio Nazionale Terremoti, Rome, Italy. ³CNRS-Sorbonne Universit e, Institut des Sciences de la Terre de Paris, Paris, France. ⁴Universit a degli Studi di Napoli Federico II, Dipartimento di Scienze della Terra, dell'Ambiente e delle Risorse, Naples, Italy. ⁵Universit a degli Studi del Molise, Dipartimento di Bioscienze e Territorio, Campobasso, Italy. [✉]email: domenico.doronzo@ingv.it

The iconic 79 CE eruption of Vesuvius was a large-scale event classified with Volcanic Explosivity Index (VEI) 6 and represents the first documented Plinian eruption, giving the name to this type of volcanic activity¹. One of the approaches in volcanology to study magma reservoir, and pre- and syn-eruptive conditions is the integration of stratigraphic, petrological, geochemical and modelling studies. Such multidisciplinary approach has been carried out for various geodynamic contexts characterised by magmatic systems of different size, fed by magmas of variable chemical composition^{2–5}. Among the studied volcanic eruptions occurred in the Neapolitan area (Southern Italy), the 79 CE eruption (also known as the autumnal “Pompeii” eruption) is one for which this integrated approach has been used^{6–10}.

Results from previous studies on the volcanic activity of Somma-Vesuvius have suggested that the magma reservoir has become shallower in the last 20 ka, from a depth of ~16 km (~18.5 ka “Pomici di Base” Plinian eruption of Mount Somma)¹¹ to a depth of ~3 km (“1944” ultra-Strombolian eruption of Vesuvius)¹². These findings have been corroborated by experimental petrology, reproducing the chemical differentiation of magma as a function of bulk MgO content in the pyroclastic products erupted from Somma-Vesuvius over time¹³. In between, the three Plinian eruptions, “Mercato” (~9 ka)¹⁴, “Avellino” (~3.9 ka)¹⁵ and “Pompeii” (79 CE)¹⁶ had a magma reservoir located at a depth of ~7.5 km, under a magma storage pressure of 175–200 MPa^{8,13,17}.

The composite sequence of the 79 CE pyroclastic products can be synthesised as follows (Fig. 1): a thin phreatomagmatic ash Eruptive Unit (EU1), a thick white-pumices magmatic fallout unit (EU2f), a thick grey-pumices magmatic fallout unit intercalated by multiple column-collapse pyroclastic current deposits (EU3f–EU3pf), a thick phreatomagmatic caldera-collapse pyroclastic current unit culminated into a locally-thick breccia unit (EU4pf–EU6), and thick phreatomagmatic pyroclastic current and fallout units (EU7–EU8). Based on stratigraphic and sedimentological analyses of the whole pyroclastic sequence, it has been possible to recognise the onset of the caldera collapse at the phase transition from magmatic (EU3) to phreatomagmatic (EU4), in which ~85% of the total magma (EU1–EU3pf) had already been erupted⁹. This occurred after the chemical transition from the white (EU2) to the grey (EU3) pumices. Indeed, the eruption was triggered by intrusion of new mafic magma, then the reservoir was subjected to progressive depressurisation (during the EU2 + EU3 Plinian phase) until collapsing⁸. On the other hand, there is some evidence that the caldera collapse could have started to nucleate a little before the end of the Plinian phase, after progressive crater enlargement^{18,19}. The petrological aspects of the 79 CE magma reservoir are given in support of the numerical modelling presented in this work (“Methods”).

Several authors developed elastic models to simulate the mechanical response of the medium to the magmatic source of the 79 CE eruption. These models are based on the finite element method (FEM) and aim at assessing the effects of the complex structure of the volcano on ground deformation, in the physical conditions that likely led to the eruption; they are summarised in Table 1. Russo et al.²⁰ and Russo and Giberti²¹ consider the mechanical instability of the volcanic edifice, adopting different shapes of the magma reservoir in 2D or 3D elastic heterogeneous media. Meo et al.²² configure a 3D model using the actual topography of Vesuvius, fixing a spherical magma reservoir at 2, 3 and 5 km depth and elastic heterogeneities of the medium, and show that the ground deformation is concentrated in the crater area. Tammaro et al.²³ improve the FEM model, by including a 3D elastic structure from tomography studies to help give a distribution of elastic and density parameters. However, there still is

a lack of studies that take into account the magma reservoir growth and the related implications for volcanic hazard. Such growth-deformation binomial is poorly known and deserves further attention⁵.

In this work, we used FEM models (see “Methods”) to simulate the magma reservoir growth and ground deformation that could have occurred prior to the 79 CE Plinian eruption of Vesuvius, as a consequence of multiple magma recharges possibly occurred in the 300 years preceding the eruption. Magma recharge from deeper sources is considered as the necessary long-term condition that precedes any volcanic eruptions²⁴. The magma reservoir, modelled with different shapes, is embedded in a viscoelastic medium consisting of a metamorphic shell around the source with lower viscosity with respect to the host rocks (Table 1 and “Methods”). The modelling is tuned with petrological and stratigraphic data on the erupted products, and is compared with paleoenvironmental records of the ground deformation around the volcano in six archaeological sites. As ground surface displacement is one of the main monitored hazard parameters at active volcanoes, this work on the well-known “Pompeii” eruption has direct implications on volcanic hazard assessment in the precursory phase(s) of Plinian eruptions.

Paleoenvironment and pre-79 CE ground deformation. In literature there is a wide documentation on the evolution of the paleoenvironment around Vesuvius, and particularly in the Sarno River Plain (Fig. 2). After the Würm glaciation (<12 ka), such evolution was characterised by marine transgression (sea level rise plus Plain subsidence) until ~5 ka before the 79 CE eruption, then the transgression velocity decreased and became less than the accretion velocity of the Plain (sedimentary plus volcanic supplies) leading to coast line progradation²⁵. In the 5 ka before 79 CE, the paleoenvironmental reconstructions are not straightforward mainly because the paleomorphology is buried by thick subaerial volcanic successions related to eruptions of Somma-Vesuvius. The largest in this period were the “Avellino” and “Pompeii” Plinian eruptions. A number of campaigns were performed with the goal of carrying out several cores through the buried sedimentary and volcanic successions in the Plain^{25–27}. More recently, other cores were carried out^{28,29} finding the presence of pre-79 CE barrier-lagoon systems sub-parallel to the current coast line.

Since the first appearance of the Charles Lyell’s “Principles of Geology” book frontispiece in 1830 showing water level changes in the Serapeo archaeological site at Campi Flegrei (Italy), geologists have focused on fossiliferous content in rocks to reconstruct the paleoenvironment³⁰. In the area around Vesuvius, palaeoecological interpretations have been based on microfaunal and meiofaunal assemblages, with particular regard to benthic foraminifers and ostracods^{26,29}. Foraminifers generally show high abundances in fully marine environments, while ostracods are important for interpretations in all aquatic environments from marine to continental. Moreover, the successions deposited in areas under the influence of volcanic activity, such as the Vesuvius case, can show alternations of fossiliferous and barren levels, which depend on depositional conditions and taphonomic processes. Marturano et al.³¹ analysed various cores in the Somma-Vesuvius apron near Pompeii, where pre-79 CE shallow marine deposits are alternated with subaerial sediments. The majority of the samples were fossiliferous, testifying both lower infralittoral zones of low-energy waters and upper infralittoral zones of high-energy waters. From other cores in the Pompeii archaeological site, Marturano et al.³² found very rare microfossils including some foraminifers and ostracods. The meiofaunal assemblages found testify an alternation of subaerial deposits

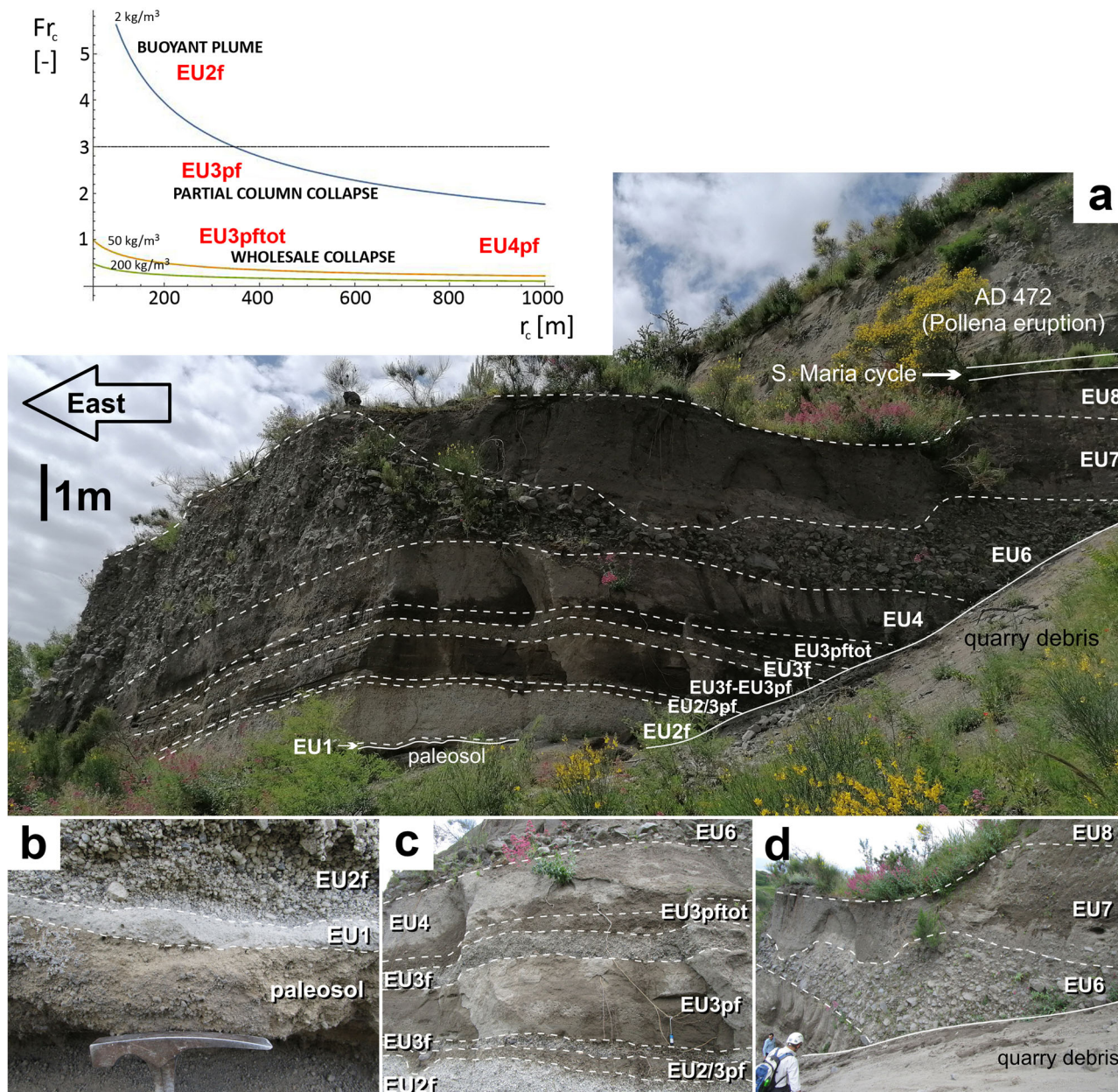


Fig. 1 Pyroclastic deposits sequence of the 79 CE Plinian eruption of Vesuvius. **a** Total sequence of the 79 CE pyroclastic deposits with each Eruption Unit (EU) reported; distance is 4.5 km from the current crater. **b–d** Details of the various EUs recognised (modified after⁹). On top, some of the main EUs inform a regime diagram (crater densimetric Froude number vs. crater radius, for three different eruption column densities) to synthesise the 79 CE eruption dynamics (modified after¹⁸).

with shallow marine sediments. From cores in the Herculaneum archaeological site, Marturano et al.³³ analysed samples that were barren or yielded very poor faunal assemblages. One level resulted relatively rich of well-diversified benthic foraminifers consisting of typical infralittoral taxa, while ostracods were even more rare, confirming the previous paleoenvironmental reconstructions.

In the central-southern sector of the Plain, the barrier-lagoon systems are characterised by the presence of a dune sequence ¹⁴C-dated at 3.8 ka before the 79 CE eruption. Instead, in the northernmost and southernmost sectors, the marine transgression (in between 7 and 12 ka) formed steep cliffs on pre-79 CE lavas around the Pompeii paleohill, all along the foothills of the southwestern flank of Vesuvius, and on the Late Pleistocene pyroclastic successions along the foothills of the northern flank of the Lattari Mountains. Another dune sequence, sub-parallel to the

previous one, has been identified at a few 100 metres closer to the sea and ¹⁴C-dated at 0.8 to 1.8 ka before 79 CE. In the sectors in between, some lagoons formed which evolved into fluvio-swamp environments. This paleoenvironmental condition seems to have lasted until the arrival of the pyroclastic products of the 79 CE eruption of Vesuvius which, besides burying the Roman towns of Herculaneum, Oplontis, Pompeii and Stabiae, led to a drastic change in the coastal environments. Because of the deposition of such pyroclastic products, the coast line and the dune sequences prograded of a few kilometres, and the low zones behind the dunes were filled^{25,29,34,35}.

In this work, these paleoenvironmental reconstructions were reviewed comparatively to depict how the morphology around Somma-Vesuvius was prior to the 79 CE eruption. Amato et al.²⁹ have provided constraints on the local vertical displacements that

Table 1 Magma reservoir models for Vesuvius.

Model geometry	Medium	Topography	Source shape	Source depth b.s.l.	Boundary conditions	Reference
Axi-symmetrical	2 layers $E = 10$ GPa $E = 40$ GPa	2D profile	Sphere Prolate spheroid	Top at 1.1 km, 2 km	Overpressure = 10 MPa Regional stress	20
Axi-symmetrical 2.5D 3D	Various configurations of the central high rigidity body (E from 10 GPa to 40 GPa)	2D profile	Prolate spheroid Cylinder Oblate spheroid	Top 1.1 km–1.7 km, centre 2 km	Overpressure = 10 MPa	21
3D	2 layers $E = 10$ GPa $E = 40$ GPa	3D	Parallelepiped	Centre at 2 km, 3 km, 5 km	Overpressure = 10 MPa	22
3D	3D from tomography (E from 10 GPa to 80 GPa)	3D	Parallelepiped	Centre at 2 km, 3 km, 5 km	Overpressure = 10 MPa	23
Axi-symmetrical 3D	Viscoelastic with thermo-metamorphic shell $E = 10$ GPa, $\nu = 0.25$ $\eta = 10^{15}$ Pa s (shell), $\eta = 10^{18}$ Pa s (host rocks)	2D profile	Prolate spheroid Sphere Oblate spheroid	Centre at 7.5 km	See Table 2	This study

Characteristics and parameters of previous and this-work magma reservoir models for Vesuvius. E is Young modulus, ν Poisson coefficient and η Maxwell viscosity.

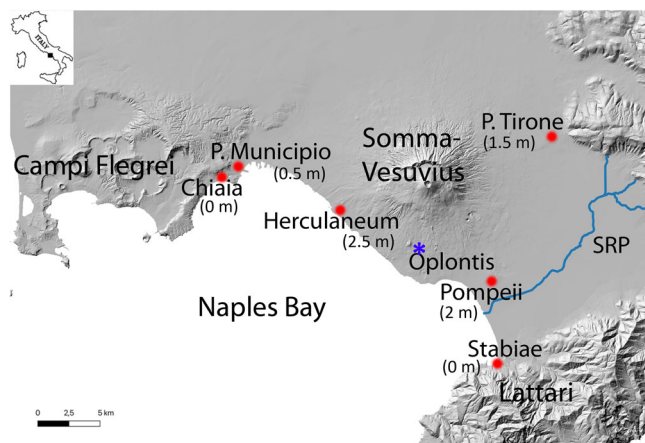


Fig. 2 Map of the Vesuvius area. The red dots represent the archaeological sites for which the ground deformation data (in brackets) are available. The blue asterisk represents the epicentre of the strongest pre-eruption earthquake occurred on 05 February 62 CE ($M = 5.1$). SRP is the Sarno River Plain. Digital Terrain Model from Tinitaly, software ArcGIS.

occurred on the ground surface prior to the event, taking into account the local degree of humification of the paleosol below the 79 CE pyroclastic deposits. With reference to the complex edifice of Somma-Vesuvius, the pre-79 CE topography in the period between the “Avellino” and “Pompeii” eruptions may be inferred from the deposit distribution³⁶. However, it is not straightforward to assume the post-“Avellino” topography as the one that preceded the 79 CE eruption, as in between the two Plinian events a number of eruptions, named AP1-6, occurred³⁷. On the other hand, the interplay among stratigraphic heights and fossiliferous vs. barren levels in the Plain successions has allowed to estimate the vertical ground deformation (uplift) that likely occurred during the whole period of magma reservoir recharge before the eruption. Such vertical ground surface displacements have been earned in five archaeological sites around Vesuvius at different distances from crater^{29,35,38,39}: Stabiae (~0 m), Pompeii (~2 m), Herculaneum (~2.5 m), Piazza Municipio, Naples (~0.5 m) and San Pasquale a Chiaia, Naples (~0 m) (Fig. 2). These archaeological sites fall in an area of 7 to 15 km radius from the current crater. Another estimate is available at Ponte Tirone, Palma Campania, where archaeological interpretations have given

an average uplift of a segment of the Roman aqueduct of ~1.5 m⁴⁰. An uncertainty of 0.5 m can be associated to the five estimates, based on recognition and interpretation of the level heights constraining the displacements^{29,39}, while an uncertainty of 1.2 m is considered for the archaeological estimate at Ponte Tirone⁴⁰. A temporal uncertainty of the order of decade can be associated to those estimates, as this (to a 100 years) is the ground deformation time span inferred from the paleosol analysis along the coast line. It is worth noting that the vertical displacements decrease with distance from the crater similarly in different directions.

Numerical modelling of the 79 CE magma reservoir growth.

3D axi-symmetric FEM models were developed to test how different initial shapes of the magma reservoir can impact on the stress conditions that likely led to the reservoir failure, and then to the 79 CE Plinian eruption of Vesuvius. The configuration of the models was based on volcanological and petrological indications of the recharge timing and magma volumes (“Methods”). In particular, three models including three different source shapes were considered: a prolate spheroid, a sphere and an oblate spheroid. The initial volume was fixed at 1.1 km³, achieving 4.4 km³ at the end of the 300-years recharge phase, which preceded the 79 CE eruption. The overpressure of the three sources was constrained by the achievement of the final magma volume. The models are viscoelastic, including a thermo-metamorphic shell in which the sources are subjected to dilatation (“Methods”).

Results of the three source expansions at the end of the 300-years recharge phase are shown in Fig. 3, while the FEM computational meshes are reported in Supplementary Fig. 1. The FEM simulations show a different evolution of the magma reservoir based on its initial shape, after achieving the same final volume for the three shapes. The prolate source has an almost radial expansion (Fig. 3a), while the sphere (Fig. 3b) and more evidently the oblate (Fig. 3c) sources grow much more vertically than horizontally. This behaviour is also documented by the displacement time-series of their axes (Fig. 4c), reporting a growth of ~1 km vertically and 100–200 m horizontally in particular for the sphere and oblate sources. This means that all the three sources tend to verticalise during the recharge phase. Also, this occurs regardless of the different overpressures generated on the wall rocks at the end of the recharge phase. Indeed, the modelling results show that for each magma reservoir

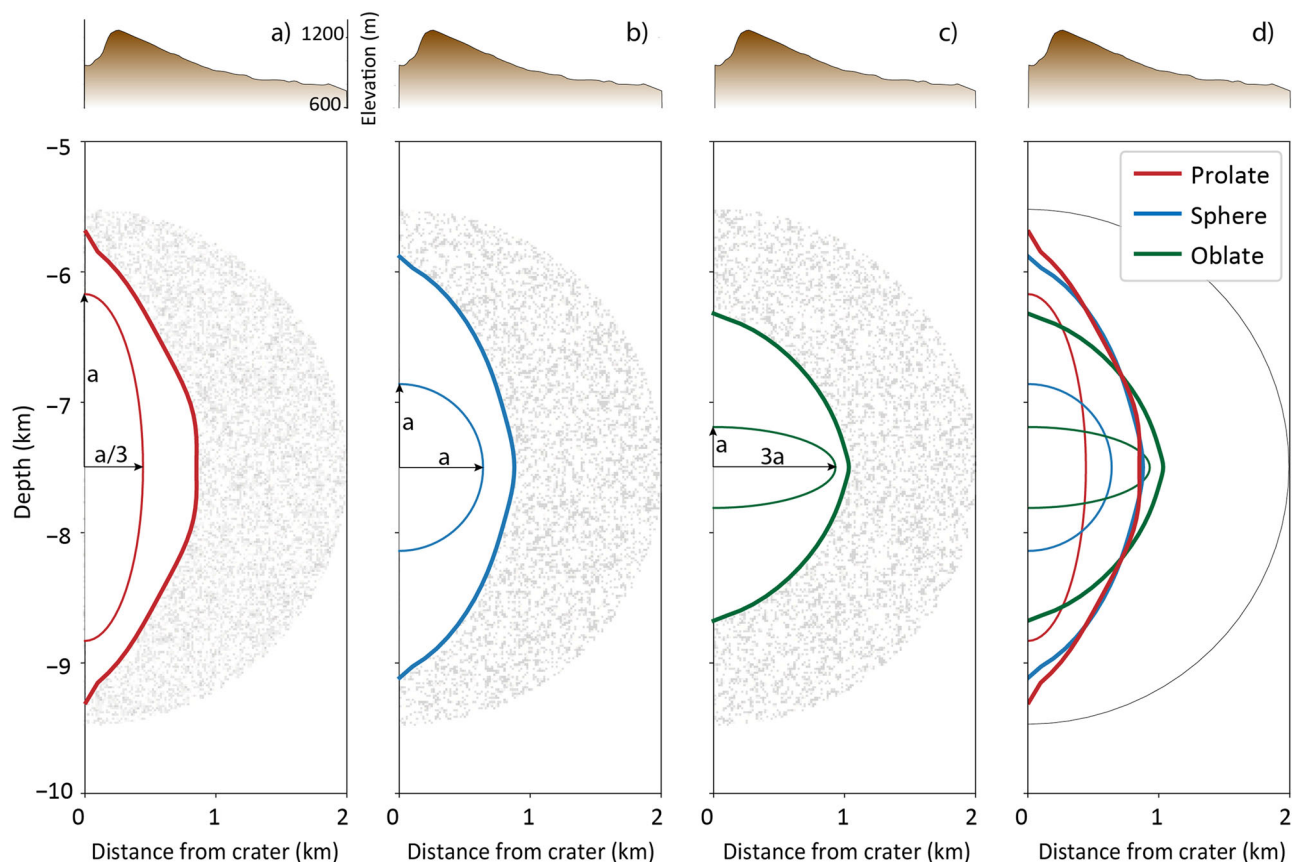


Fig. 3 Models of the 79 CE magma reservoir in this work. Magma reservoir simulated by FEM in the viscoelastic medium. **a** Red, prolate spheroid; **b** Blue, sphere; **c** Green, oblate spheroid; details are reported in Table 2. The three sources have the same initial volume (1.1 km^3 , thin lines) and expand achieving the same final volume after 300-years recharge (4.4 km^3 , thick lines). The grey shaded area is the viscoelastic shell with lower viscosity with respect to the host rocks. **d** Comparison among the initial (thin lines) and final (thick lines) volumes. The shell boundary is reported with a thin black line. The topography from the central crater is reported on top (horizontal in scale, vertical not to scale).

Table 2 Models of the 79 CE magma reservoir in this work.

Model	a_{a_H} (m)	a_{a_V} (m)	a_H/a_V	$b\Delta P_{\max}$ (MPa)
Prolate	443	1330	0.33	100
Sphere	640	640	1	85
Oblate	930	310	3	50

Characteristics of the three models considered in the present work.

a_{a_H} is horizontal semi-axis, a_{a_V} vertical semi-axis.

$b\Delta P_{\max}$ Maximum overpressures attained at the end of the cumulative recharge phase.

shape simulated, the overpressure required for the expansion is different (Table 2). The oblate source needs ~ 50 MPa, half of the overpressure of the prolate source (~ 100 MPa), to yield the same final volume.

The vertical ground surface displacements amount to 4–5 m in the crater area at the end of the recharge phase (Fig. 4a). Even if the FEM models were calibrated only considering the magma reservoir growth (from 1.1 km^3 to 4.4 km^3), the ground deformation simulated is in agreement with the six paleoenvironmental and archaeological elevation changes that preceded the 79 CE eruption (Paleoenvironment and pre-79 CE ground deformation), as shown in Figs. 4a and 5. Indeed, the chi-squares computed for the prolate, sphere and oblate models are 0.6, 0.7 and 0.6, respectively. The time-series at the site closest to the crater (Fig. 4b), Herculaneum, shows similar behaviour for the models considered, reporting the slight scaling among the three models as in the patterns of Fig. 4a. The wavy pattern is

modulated by separate magma inputs, which is reported in terms of the overpressure variation curve in the bottom of the figure panel (Fig. 4b). During recovery after each batch of magma enters the reservoir, there is no subsidence due to viscoelastic effects. The oblate source approaches a more continuous trend with respect to the step-like trend of the sphere and prolate sources. This is also confirmed by the time-series of vertical and radial expansion of the magma reservoir, in terms of upward expansion of the vertical semi-axis and radial expansion of the horizontal semi-axis (Fig. 4c).

Discussion

The FEM models allow to investigate the binomial between the 79 CE magma reservoir growth and pre-eruption ground deformation. Despite the different initial source shapes, all three models achieve a vertically-elongated shape at the end of the simulations (Fig. 3d). In particular, both the prolate and spherical sources almost attain the same final shape. The felsic magma and the top of the grey magma were H_2O -saturated, at a storage/crystallisation pressure ranging from 175 to 200 MPa, and corresponding to a magma reservoir located at ~ 7.5 km depth with an initial vertical extent of ~ 500 m¹⁷. On the other hand, no petrological constraints are available for the overall extent of the 79 CE magma reservoir. For this, and considering that the felsic magma represents 1/3 of the total erupted magma volume, Balcone-Boissard et al.⁸ have hypothesised a further vertically-elongated magma reservoir. Such shape fits also well with the syn-eruptive saturation of the deepest part of the grey magma, correlating with

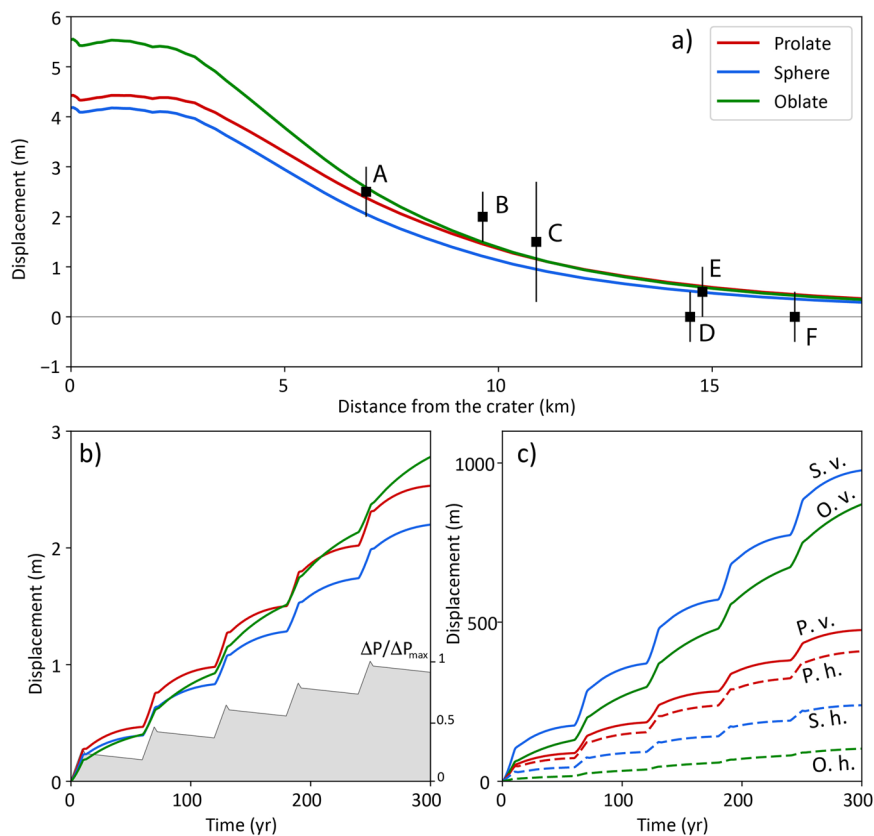


Fig. 4 Uplift after the 79 CE magma reservoir growth. **a** Vertical displacements on the ground surface (uplift) at the end of the 300-years mafic magma injection phase, related to the three models considered. The black squares represent the archaeological data (A = Herculaneum, B = Pompeii, C = Ponte Tirone, D = Stabiae, E = Piazza Municipio, F = San Pasquale a Chiaia) with the associated uncertainty. **b** Time-series of the vertical displacement in Herculaneum (the data site closest to the crater, located at a distance of ~7 km); colours as in **(a)**. On bottom, it is reported the normalised overpressure variation history over 300 years due to the magma batches entering the reservoir (shaded area; specific $\Delta P/\Delta P_{\max}$ for each model is reported in Table 2). **c** Time-series of vertical and radial expansion of the three sources (O oblate, S sphere, P prolate) with colours as in **(a)** considering the upward expansion of the vertical semi-axis (v.) and radial expansion of the horizontal semi-axis (h.).

the onset of the total Plinian column instability^{9,41}, and easiest to achieve by a prolate shape with respect to an oblate one, and confirming that the dynamics inside and outside the volcano are intimately coupled through crater conditions¹⁸ (Fig. 1).

The similar vertical shape for the three models is attained regardless of the different overpressures generated on the wall rocks. Indeed, the modelling results show that for each magma reservoir shape simulated, the overpressure required for the expansion is different (Table 2). The prolate source shows the highest overpressure build up on its walls at the end of the recharge phase, which means that it has limited capabilities to sustain the internal overpressure build up. The oblate source requires half of the overpressure of the prolate source to yield the same final volume. This is not surprising since sill-like sources, penny-shaped cracks⁴², and in general sources with horizontal extent larger than vertical one generate larger volume variations with respect to more spherical shapes, given the same overpressure^{5,43}. Conversely, in this work the volume variation is kept constant (from 1.1 km³ to 4.4 km³), while the involved overpressures vary depending on the source shape, although comparisons are not straightforward since the expansion occurs in a 3D viscoelastic medium.

Given a magma reservoir shape, the maximum overpressure that can be achieved depends on magma supply rate^{24,44}. For the 79 CE eruption, the magma supply rate is averaged by the erupted magma volume over recharge time, and such average represents a source of uncertainty for the FEM modelling. The average magma

supply rate in the models is of ~0.01 km³/year, which is within the highest limit for continental volcanoes involving relatively mafic magma entering the high-silica high level system^{45–48}. Lower magma supply rates (~0.005 km³/year) might have been occurred at Vesuvius, but in this case, a similarity between the 79 CE Plinian eruption and smaller eruptions of the recent activity (1872–1944) in open conduit conditions should be assumed⁴⁹. The models did not take into account the eruption dynamics^{5,19}, which has already been investigated with a stratigraphic-modelling integrated approach⁹, nor take into account the thermodynamic state of the reservoir^{47,50}.

The three models of the magma reservoir (oblate, sphere and prolate sources) show slightly different spatio-temporal trends for the ground deformation after 300-years stepwise recharge. In general, the oblate case gives vertical ground surface displacements larger than the prolate and sphere cases, but the absolute values are not drastically different for all the three cases (4–5 m maximum values), particularly beyond a few kilometres from the crater (~1–3 m). The simulated uplift deformations fit the displacement data within uncertainty from the paleoenvironmental analysis in the reference archaeological sites (Figs. 4 and 5). A similar modelling-paleogeodetic comparison has recently been done for Laguna del Maule, Chile⁹. In terms of ground uplift velocity, a time-averaged (over 300 years) maximum value of ~1.7 cm/year is calculated near the crater, while lower values are calculated gradually further away, as expected. On the other hand, such velocities are higher at each grey magma recharge event

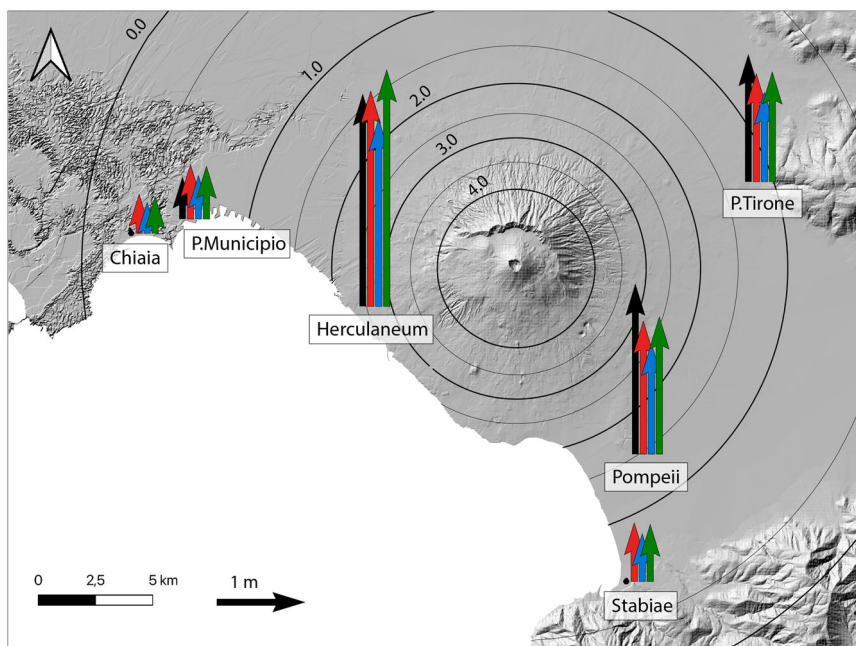


Fig. 5 Comparison between archaeological and modelling results. Comparison between archaeological elevation changes (black arrows) and vertical ground surface displacements for the prolate (red), sphere (blue) and oblate (green) sources in the six reference sites. The actual location of the site corresponds to the position of the paleoenvironmental data. The vertical displacement for the prolate source is reported with contour lines (thick line 1-m iso-deformation, thin line 0.5-m iso-deformation). It is worth noting the areal extent of the contour lines up to the main geological complexes around Somma-Vesuvius: Campi Flegrei volcano to the west, Lattari Mountains to the southeast, Apennine Chain in the Campanian Plain to the northeast. Digital Terrain Model from Tinitaly, software ArcGIS.

(over <60 years) because the ground deformation is not constant over time. For example, the uplift velocity at Herculaneum during each magma injection is twice the abovementioned value. The ground surface displacements after each injection show trends that modulate the gentle overpressure drop due to viscoelastic effects (see slopes in Fig. 4b).

Magma storage pressure can be constrained by melt inclusion studies as described in “Methods”, while the overpressure generated by the mafic magma injections is constrained by FEM. Although the three models attain similar residual misfits in terms of ground deformation, the differences for the three analysed cases in terms of overpressure are larger, with important volcanic hazard implications. The end member overpressures are of 50 and 100 MPa (with a factor 2) for the oblate and prolate cases, respectively (Table 2). Considering that ground deformation is one of the main surveillance parameters at active volcanoes, it is not straightforward to identify a direct relationship between deformation and the characteristics of future eruptions. In fact, the relationship is complicated since different magma reservoir shapes can cause similar ground deformations while having significantly different magma overpressures. This, in turns, may lead to different eruption styles and also to different erupted (or eruptible, in case of a future event) magma volumes^{51–53}. Clearly, the eruption probability, style and size depend on several factors including magma overpressure, volatile elements content, magma reservoir depth, and regional/local stress regime^{54,55}.

Therefore, it is not possible to directly associate the ground deformation to a specific eruption style and size, or infer how close the reservoir is to its wall failure only based on this surveillance parameter. The involved overpressure has a first-order role in eruption probability and eruption evolution, because not all overpressure values lead to eruption nor, in case, to the same type of eruption. With reference to the 79 CE Plinian eruption, given the magma water content and magma recharge rate, and the initial magma volume of $\sim 1 \text{ km}^3$ growing to 4.4 km^3 ,

thermo-mechanical simulations suggest that pressures within 150–250 MPa imply favourable conditions to long-lived and eruptible bodies⁵². Below these values, the reservoir conditions are favourable to volcanic eruptions, but the magmatic system cannot build up to a significant size, while above are favourable to large plutonic bodies. The magma storage pressure in the upper part of the reservoir is constrained to be 175–200 MPa (“Methods”), which coupled with the modelled overpressures gives a value of pressure favourable to large volcanic eruptions. Given the same final magma volume achieved and similar ground deformation pattern, the prolate magma reservoir shows an overpressure build up more likely to the achievement of an impending eruption state. It is worth remarking that the entire overpressure range from the simulations (50–100 MPa) implies favourable conditions for dyke nucleation feeding a silicic eruption^{45,56,57}. Such nucleation also depends on the internal thermodynamic state and tectonic conditions of the reservoir^{19,50}. A direct implication of these simulations for volcanic hazard assessment is that it is not possible to hypothesise the achievement of the stress limit of the magma reservoir walls, due to the lack of information on its actual source shape.

It is worth noting that complex models were implemented in the present work, in order to also include the topography and non-homogeneous viscoelastic properties of the medium. On the other hand, the number of parameters used in the simulations was limited, considering the medium elastically-homogeneous and with two viscosities, one for the thermo-metamorphic shell and the other for the host rocks. However, these models are not unique and other configurations may be equally possible, also considering the uncertainties associated to an eruption of 2000 years ago. For example, the calculated overpressures may result overestimated and might be lowered by introducing a thermal model impacting on the interplay between the overpressure and stress evolution⁵⁸. Conversely, the presence of a poroviscoelastic crystal mush in the reservoir might cause a prolonged

deformation, and consequently lower overpressures might be required to achieve the same final volume⁵⁹.

In the present work, it is shown an example of how a well-studied past eruption can help improve the interpretation of the unrest features at active explosive volcanoes, particularly those like Vesuvius that may repeat, based on their volcanological history, a Plinian or in general a large-scale (including sub-Plinian) eruption. These considerations on the uncertainty of the actual magma reservoir shape and related effects should be taken into account in the surveillance activities. Indeed, a consequence of the present modelling results is that even significant ground deformations may not lead to an eruption. However, it is also true that such deformations may at the same time lead to an eruption, meaning that the actual time span for an eruption to become irreversible can be much shorter than each recharge event of the magma reservoir, i.e. « 60 years for the modelled 79 CE eruption. It is worth noting that the major earthquake occurred in 62 CE at Vesuvius ($M = 5.1$) was not followed by immediate eruption; the latter occurred 17 years later. In contrast, for the 3.6 ka “Minoan” Plinian eruption of Santorini (Greece), one (or more) major destructive earthquake(s) occurred <1 year before the phreatomagmatic opening phase⁶⁰. For example at Tenerife (Spain), timescales from a month to hours have been inferred for magma mixing to occur prior to sub-Plinian to caldera-forming eruptions^{4,61}. This is in agreement with Balcone-Boissard et al.¹⁷, who have found that magma mingling might have shallowly occurred in the feeder conduit of the 79 CE eruption. At Kizimen (Russia), timescales of ~1.5 years have been found for magma mixing to occur prior to an extrusive-explosive eruption, in concomitance with a seismic crisis, then the reservoir was destabilised⁶². For the “1631” sub-Plinian eruption of Vesuvius, it has been reported by historical chronicles (without quantification) that a significant and visible uplift of the crater bottom occurred about a month before the eruption, while various intracrater rockfalls started about a year earlier⁶³. By further widening discussion, at Kilauea (United States) which is a volcano very different from Vesuvius, timescales of ~3 months have been found for unrest and inflation to occur prior to a lava fountaining eruption, while the magma recharge into the reservoir started even well before⁶⁴. At Krafla (Iceland), another volcano different from Vesuvius, magma accumulated in the reservoir generating a ground inflation for timescales usually <1 year before having dykes propagation in basaltic fissural eruptions⁶⁵. At Chaitén (Chile), timescales <1 year have been found for ground deformation to occur prior to the sub-Plinian phase of a complex rhyolitic eruption ended with a dome extrusion, which was driven by a combination of magma buoyancy and overpressure⁶⁶.

From the surveillance viewpoint at active volcanoes, the classical multiparametric monitoring networks should therefore be complemented with techniques, physics-based and event tree models aimed at forecasting the possible impending eruption state related to dyke propagation^{24,44,67}, as well as forecasting the eruption style and size on time^{5,52,53,68}. It is known that ground deformation generally accompanies subsurface gravity variations due to magma intrusion. However, the deformation-gravimetric relationships are not direct because depend on a number of factors, including magma reservoir shape and magma compressibility⁶⁹. In general, larger gravity variations are typical of oblate sources, while prolate and sphere sources yield more similar variations to each other (at the same conditions). Such variations are larger in proximal areas⁶⁹, similarly to the vertical displacement patterns simulated (Fig. 4a). Geophysical studies of the seismic structure underneath Vesuvius reveal several important features, both at shallow depth and down to 15 km^{70,71}. In particular, a high- V_p and high- V_s body located at 3–5 km depth can be interpreted as unerupted solidified fractionated material, which accumulated in a shallow-

intermediate reservoir. On the other hand, from receiver function analysis, there is evidence of a low- V_s zone between 5.5 and 8.5 km depth⁷¹, compatible with a fluid-phase stockage volume at the same location of the reservoir modelled in the present work, and in agreement with petrological studies⁷². Such volume is therefore still present and large enough to be capable of future eruptions, but this will also depend on the evolving magma reservoir shape. In light of the present work, the large-scale eruption of Hunga Tonga-Hunga Ha’apai (Tonga) occurred on 15 January 2022 confirms that the absence of precursory evidence is not an evidence of precursory absence, and that the monitoring-modelling-volcanological integrated approach at active volcanoes is the key for short- to long-term eruption forecasting.

Conclusions

As the differently-shaped (prolate, spherical, oblate) modelled reservoir grows and builds up its overpressure, the time-dependent uplift values are not drastically different among shapes, while the overpressure values differ significantly and these directly affect the eruption probability. This implies that some switch to the impending 79 CE eruption state might have occurred on the short-term, giving a few pre-alarm to people still populating the Vesuvius area until the first eruption phases. More data (historical, geomorphological and geochemical) will eventually refine a retrospective forecasting for this Plinian eruption. On the other hand, geophysical (tomographic, gravimetric), volcanological and geochemical/petrological integrated studies are necessary on the long-term to better understand the current geological structures (including magma reservoir shape) underneath Vesuvius prior to the next eruption. It is to remark the importance of multiparametric surveillance at active volcanoes like Vesuvius, as this work is applied to investigate the ground deformation, but a combination with other surveillance parameters (e.g., seismic, geochemical) is necessary to forecast an impending eruption state on the short-term.

Methods

Magma reservoir and magma recharge. The total volume of the magma emitted during the 79 CE Plinian eruption has been estimated at 4.4 km³ Dense Rock Equivalent (DRE), of which ~1 km³ was erupted as white pumices, ~2.7 km³ as grey pumices and ~0.7 km³ as phreatomagmatic products^{16,73}. Doronzo et al.⁹ have recently calculated an extra volume of 0.5 km³ over the grey pumices, by including ultra-distal findings of the 79 CE cryptotephra recognised in Sicily and in the Adriatic Sea, and off the coast of Crete. A main stratigraphic feature of the 79 CE fallout deposits emplaced during the Plinian phase is a marked change of chemical composition and juvenile clast density passing from the white (EU2f) to the grey (EU3f) pumices^{74,75}. The white pumices are K-phonolitic (~56% SiO₂, ~9% K₂O) and have a density of ~600 kg/m³, while the grey pumices are K-tephri-phonolitic (~54% SiO₂, ~8% K₂O) and have a more variable density ranging from ~500 to 1300 kg/m³³⁸. Such variations have been ascribed to a compositional zonation of the 79 CE magma reservoir⁶ which, along with variations of volatile contents, were responsible for fluctuations of the eruption column height and magma discharge rate⁷⁴.

Cioni et al.⁶ and Balcone-Boissard et al.⁸ have established the temperatures of the two chemically-distinct magmas involved in the 79 CE eruption. The more felsic magma (white magma) was at a temperature of ~850 °C, while a more mafic magma entering the reservoir system was at a temperature of ~1000–1200 °C. The coexistence of the two magmas possibly produced a thermal zonation in the magma reservoir imposed by the presence of the felsic magma at the top of the reservoir, and by repeated injections of the deeper and more mafic magma^{76,77}. The grey pumices resulted from syn-eruptive mixing of these two (felsic and mafic) end member magmas, giving rise to the grey magma⁸. The white and grey magmas also differ in terms of vesicularity and crystallinity as a consequence of the ascent-driven degassing, as identified by textural studies^{8,78}. Cioni et al.⁷⁵ have estimated that during the different phases of the eruption ~25–30% of the total magma was erupted as white pumices, while ~70–75% as grey pumices, and also that the white pumices resulted from tapping of a pre-existing k-phonolitic (white) magma as a possible residue of the “Avellino” Plinian eruption. The grey magma had a K-tephri-phonolitic composition, variable ⁸⁷Sr/⁸⁶Sr isotopic ratio (0.70748–0.70757), high temperature (1000–1100 °C), low dynamic viscosity (150–170 Pa s), and relatively high density (2350–2400 kg/m³). Similar results have been obtained by

Marianelli et al.⁷⁶, who analysed Melt Inclusions (MIs) in olivine and diopside crystals from the products of various Vesuvius eruptions.

Balcone-Boissard et al.¹⁷ have focused on the pumice-fallout deposits formed during the 79 CE eruption (EU2f and EU3f). These authors performed several estimates of H₂O content in MIs using the “by difference” method, and compared the results with those available in the literature obtained by different techniques (FTIR, SIMS). In such pyroclastic products, the sanidine crystals display the most differentiated MIs composition, and have H₂O contents ranging from 3.5 to 6.5 wt %. The major elements content of MIs in pyroxene crystals spans a wider range, which extends towards poorly differentiated melt composition, featured by H₂O contents ranging from 1 to 5 wt%. MIs in leucite crystals display the lowest H₂O content, that is 0.7–2.6 wt%. These data have been interpreted as evidence of shallow syn-eruptive magma mingling between the felsic and mafic magmas during ascent in the feeder conduit. Balcone-Boissard et al.¹⁷ have suggested that the felsic magma was stored in the upper part of the reservoir and saturated at pressures of 175–200 MPa, corresponding to ~7.5 km depth, considering an H₂O content of 5 wt%. Similar results have been obtained by considering Cl solubility⁷² and bulk MgO content¹³. The mafic magma was stored just below the felsic one, but no constraints have been given on the vertical extent of the deeper reservoir. Cioni et al.⁷⁵ have suggested an ellipsoidal or cylindrical geometry and a minimum volume of ~5 km³ for the magma reservoir that fed the 79 CE Plinian eruption, taking into account ~0.6 km³ of unerupted mafic cumulates; the suggested vertical extent of the reservoir is 1 to 1.5 km.

Assuming that fractional crystallisation, dissolution-regrowth, recharge and mixing all occurred before the 79 CE eruption, the timescales of such processes can be determined by investigating diffusion profiles within individual crystals. Morgan et al.⁷⁷ have identified distinct recharge events based on abrupt changes in Barium concentration at the rim of the zoned sanidine crystals. The two most recent of these events could have occurred 15 and 20 years before the eruption, while other two events 30 and 80 years before, suggesting that at least four episodic magma recharge inputs occurred at Vesuvius in the last century prior to this Plinian event. From the seismic viewpoint, at least three major earthquakes have been described in historical chronicles; these occurred in 37 CE ($M = 4.0\text{--}4.5$), on 05 February 62 CE ($M = 5.1$), and in 64 CE ($M = 3.5\text{--}4.0$)³³. Therefore, at least one of those recharge events might have been related to the 62 CE seismic event⁷⁷, possibly causing local high stress levels in the crust as documented by the intense pre-eruption seismic activity. A significantly higher frequency of relatively small seismic events (with respect to background) might have occurred some weeks to months before the 79 CE eruption⁶⁰. Geochemically, a pre-eruption degassing of S and CO₂ might have occurred on the long-term, with a few tens of Mt over the total recharge period⁷⁹. However, given the available data on this past eruption, not more (e.g., quantitative seismic frequency, daily degassing fluxes) can be stated for a retrospective forecasting of the eruption.

Volcanological studies have highlighted the occurrence of at least six eruptive events in the time span between the two last Plinian eruptions of Vesuvius (“Avellino” to “Pompeii”), which are the AP1-6 eruptions³⁷. These eruptions were fed by magmas chemically similar to the last erupted magma during the “Avellino” eruption, as well as to the first erupted (white) magma during the “Pompeii” eruption. Considering this, it may be assumed some AP6 magma as the possible residue in the reservoir feeding the 79 CE eruption. Therefore, the cumulative recharge period can reasonably be assumed in between the AP6 (217 BC)¹⁴ and 79 CE eruptions. In order to configure the models and for the sake of simplicity, a full period of 300-years recharge and five discrete recharge events (one every 60 years, including the AP6-derived first one) were thus considered. It was not possible to exactly synchronise the recharge events of Morgan et al.⁷⁷ with the historical seismic events, also because the latter were obviously not recorded by instruments. Such simplification does not preclude the goal of the modelling, which is to compare different magma reservoir shapes and their effects, given the 300-years recharge and the 79 CE erupted magma volume. The simplified frequency of recharge in the models is not surprising², and has to be considered as long-lasting with respect to the much shorter switch to the impending state of a large-scale eruption (see main text).

FEM simulations of the magma reservoir. FEM models were developed considering three scenarios in which the magma reservoir is centred at 7.5 km depth, and assuming three different shapes with the same initial volume of 1.1 km³: (1) a prolate spheroid with aspect ratio 1:3; (2) a sphere with aspect ratio 1:1; and (3) an oblate spheroid with aspect ratio 3:1. These are end-member and simplified configurations among the possible ones, and are representative of early stages of the magma reservoir. Their specific characteristics are reported in Table 2. The FEM models are 3D axi-symmetrical and include the average eastward topographic profile of Mount Somma from the central crater at easting 451.6 Km and northing 4519 Km UTM zone 33. The topography of the post-AP6 and pre-79 CE eruptions edifice is not exactly known, but this does not preclude the interpretation of the FEM modelling results. Such topography reaches 1220 m a.s.l., and approaches 70–80 m altitude at a distance of 7–8 km from the symmetry axis. The computational domain is 50 km × 50 km and is made of 3158 quadrilateral elements, it has an axi-symmetrical geometry and a resolution of 100–150 m close to the source and to the prominent surface topography, and degrading to the periphery. The bottom of the domain has zero vertical displacements as boundary condition.

Under the crustal conditions of long-term recharge, the rock rheology can be represented by a viscoelastic body⁸⁰ to describe the non-instantaneous viscous stress response. The viscoelastic rheology of the magma reservoir walls controls the stress distribution and therefore the overpressure accumulation on the wall rocks, preventing dyke nucleation^{48,56}. The FEM medium was defined as viscoelastic (Maxwell model), with a shell of 2-km radius around the magma reservoir centre. Such shell could have developed during thermo-metamorphic processes that affected the host rocks for a long time before the 79 CE eruption. Thermo-metamorphic assimilation and solidification of the mafic magma entering the system took place within this shell surrounding the reservoir. The viscoelastic medium is capable of accommodating the sudden arrivals of new magma in the reservoir. The host rock viscosity beyond the shell boundary was assumed equal to 10¹⁸ Pa s (typical crustal value for volcanic areas, and specifically constrained by post-seismic relaxation in the region)^{81,82}, while the ductile shell was characterised by a viscosity of 10¹⁵ Pa s^{83–85}. This latter value is in agreement with the temperature-dependent viscosity from the Arrhenius formulation:

$$\eta = A_D e^{(E/RT)} \quad (1)$$

where Dorn parameter $A_D = 10^9$ Pa s, activation energy $E = 1.2 \times 10^5$ J mol⁻¹⁸⁶, and R is the universal gas constant (8.314 J mol⁻¹ K⁻¹), considering a temperature of 1250 K (corresponding to 977 °C) for the mafic magma. In order to limit the unknowns, the elastic parameters of the models are homogeneous (Table 1), with Young modulus equal to 10 GPa and Poisson coefficient equal to 0.25^{45,52}.

In the three simulations, the initial volume of the magma reservoir was 1.1 km³, representing the felsic differentiated magma^{9,16}. This magma is considered as the possible residue of the magma that fed the AP6 eruption³⁷, and was emplaced at crustal depth ~300 years before the 79 CE eruption. The magma reservoir was progressively recharged by the mafic magma, following the petrological and stratigraphic reconstructions⁸. Such mafic inputs were discrete events in agreement with Morgan et al.⁷⁷, instead of steady-state supply⁷⁵. Based on the petrological and volcanological indications, five magma inputs were considered in the FEM models as refilling of the post-AP6 reservoir, following the results of the diffusion chronology. Each single magma injection was considered to last for a few years, causing sudden increase of the magma reservoir volumes. The reservoir walls were subjected to a stress build up that was only partially recovered soon after the end of the injection and until a new input took place. Based on the volume of the 79 CE pyroclastic deposits and their density, the constraint of the simulations is final volume of the magma reservoir prior to the eruption, at least 4.4 km³, and the overpressure of each model scales accordingly as reported Table 2. We used the MSC-Marc® software to carry out the FEM simulations. The final volume variation was computed by numerical axi-symmetrical integration given the final source boundary. The simulation results were constrained with archaeological data of the pre-79 CE uplift in the Vesuvius area⁸⁷.

Data availability

All archaeological data used for constraining the models are provided in the paper. The data are also available at <https://doi.org/10.5281/zenodo.7970464>.

Code availability

MSC-Marc® software was used for this work and is commercially available. The elastic parameters of the models were used to calculate numerically the uplift results.

Received: 13 December 2022; Accepted: 5 June 2023;

Published online: 14 June 2023

References

- Cioni, R. et al. Assessing pyroclastic fall hazard through field data and numerical simulations: example from Vesuvius. *J. Geophys. Res.* **108**, B22063 (2003).
- Matthews, N. E., Huber, C., Pyle, D. M. & Smith, V. C. Timescales of magma recharge and reactivation of large silicic systems from Ti diffusion in quartz. *J. Petrol.* **53**, 1385–1416 (2012).
- Cashman, K. V. & Giordano, G. Calderas and magma reservoirs. *J. Volcanol. Geotherm. Res.* **288**, 28–45 (2014).
- Marti, J. et al. Controls of magma chamber zonation on eruption dynamics and deposits stratigraphy: the case of El Palomar fallout succession (Tenerife, Canary Islands). *J. Volcanol. Geotherm. Res.* **399**, 106908 (2020).
- Townsend, M. Linking surface deformation to thermal and mechanical magma chamber processes. *Earth Planet. Sci. Lett.* **577**, 117272 (2022).
- Cioni, R., Marianelli, P. & Santacroce, R. Thermal and compositional evolution of the shallow magma chambers of Vesuvius: evidence from

- pyroxene phenocrysts and melt inclusions. *J. Geophys. Res.* **103**, 18277–18294 (1998).
7. Gurioli, L., Zanella, E., Pareschi, M. T. & Lanza, R. Influences of urban fabric on pyroclastic density currents at Pompeii (Italy): flow direction and deposition (part I). *J. Geophys. Res.* **112**, B05213 (2007).
 8. Balcone-Boissard, H., Boudon, G. & Villemant, B. Textural and geochemical constraints on eruptive style of the 79 AD eruption at Vesuvius. *Bull. Volcanol.* **73**, 279–294 (2011).
 9. Doronzo, D. M. et al. The 79 CE eruption of Vesuvius: a lesson from the past and the need of a multidisciplinary approach for developments in volcanology. *Earth Sci. Rev.* **231**, 104072 (2022a).
 10. Doronzo, D. M., Di Vito, M. A., de Vita, S., Ricciardi, G. P. & Sparice, D. Reply to the comment on “The 79 CE eruption of Vesuvius: a lesson from the past and the need of a multidisciplinary approach for developments in volcanology” by Doronzo et al., 2022 (Earth-Science Reviews 231, 104072). *Earth Sci. Rev.* **236**, 104267 (2023).
 11. Landi, P., Bertagnini, A. & Rosi, M. Chemical zoning and crystallization mechanisms in the magma chamber of the Pomici di Base plinian eruption of Somma-Vesuvius (Italy). *Contrib. Mineral. Petrol.* **135**, 179–197 (1999).
 12. Fulignati, P., Marianelli, P., Métrich, N., Santacroce, R. & Sbrana, A. Towards a reconstruction of the magmatic feeding system of the 1944 eruption of Mt Vesuvius. *J. Volcanol. Geotherm. Res.* **133**, 13–22 (2004).
 13. Scaillet, B., Pichavant, M. & Cioni, R. Upward migration of Vesuvius magma chamber over the past 20,000 years. *Nature* **455**, 216–219 (2008).
 14. Santacroce, R. et al. Age and whole rock–glass compositions of proximal pyroclastics from the major explosive eruptions of Somma-Vesuvius: a review as a tool for distal tephrostratigraphy. *J. Volcanol. Geotherm. Res.* **177**, 1–18 (2008).
 15. Di Vito, M. A. et al. The Afragola settlement near Vesuvius, Italy: the destruction and abandonment of a Bronze Age village revealed by archaeology, volcanology and rock-magnetism. *Earth Planet. Sci. Lett.* **277**, 408–421 (2009).
 16. Sigurdsson, H., Carey, S., Cornell, W. & Pescatore, T. The eruption of Vesuvius in A.D. 79. *Natl Geogr. Res.* **1**, 332–387 (1985).
 17. Balcone-Boissard, H., Villemant, B., Boudon, G. & Michel, A. Non-volatile vs volatile behaviours of halogens during the AD 79 plinian eruption of Mt. Vesuvius. *Earth Planet. Sci. Lett.* **269**, 66–79 (2008).
 18. Doronzo, D. M., Giordano, G. & Palladino, D. M. *Energy facies*: a global view of pyroclastic currents from vent to deposit. *Terra Nova* **34**, 1–11 (2022b).
 19. Gregg, P. M., de Silva, S. L., Grosfils, E. B. & Parmigiani, J. P. Catastrophic caldera-forming eruptions: thermomechanics and implications for eruption triggering and maximum caldera dimensions on Earth. *J. Volcanol. Geotherm. Res.* **241–242**, 1–12 (2012).
 20. Russo, G., Giberti, G. & Sartoris, G. Numerical modeling of surface deformation and mechanical stability of Vesuvius volcano, Italy. *J. Geophys. Res.* **102**, 24785–24800 (1997).
 21. Russo, G. & Giberti, G. Numerical modeling of surface deformations on Mt. Vesuvius volcano (Italy) in presence of asymmetric elastic heterogeneities. *J. Volcanol. Geotherm. Res.* **133**, 41–54 (2004).
 22. Meo, M., Tammaro, U. & Capuano, P. Influence of topography on ground deformation at Mt. Vesuvius (Italy) by finite element modelling. *Int. J. Non Linear Mech.* **43**, 178–186 (2008).
 23. Tammaro, U., Riccardi, U., Romano, V., Meo, M. & Capuano, P. Topography and structural heterogeneities in surface ground deformation: a simulation test for Somma-Vesuvius volcano. *Adv. Geosci.* **52**, 145–152 (2021).
 24. Caricchi, L., Townsend, M., Rivalta, E. & Namiki, A. The build-up and triggers of volcanic eruptions. *Nat. Rev. Earth Environ.* **2**, 458–476 (2021).
 25. Cinque, A. La trasgressione versiliana nella Piana del Sarno (Campania). *Geogr. Fis. Din. Quat.* **14**, 63–71 (1991).
 26. Barra, D. et al. Evoluzione geologica olocenica della piana costiera del Fiume Sarno (Campania). *Mem. Soc. Geol. Ital.* **4422**, 255–267 (1989).
 27. Pescatore, T., Senatore, M. R., Capretto, G., Lerro, G. & Patricelli, G. Ricostruzione paleo ambientale delle aree circostanti l’antica città di Pompeii (Campania, Italia) al tempo dell’eruzione del Vesuvio del 79 d.C. *Boll. Soc. Geol. Ital.* **118**, 243–254 (1999).
 28. Vogel, S. & Maerkerl, M. Reconstructing the Roman topography and environmental features of the Sarno River Plain (Italy) before the AD 79 eruption of Somma-Vesuvius. *Geomorphology* **115**, 67–77 (2010).
 29. Amato, V., Aiello, G., Barra, D., Infante, A. & Di Vito, M. A. Nuovi dati geologici per la ricostruzione degli ambienti marino-costieri del 79 d.C. a Pompeii. *Rivista di Studi Pompeiani* **32**, 103–111 (2021).
 30. Lyell, C. *Principles of Geology* 528 (Penguin Classics, 1998).
 31. Marturano, A., Aiello, G. & Barra, D. Evidence for Late Pleistocene uplift at the Somma-Vesuvius apron near Pompeii. *J. Volcanol. Geotherm. Res.* **202**, 211–227 (2011).
 32. Marturano, A. et al. Evidence for Holocene uplift at Somma-Vesuvius. *J. Volcanol. Geotherm. Res.* **184**, 451–461 (2009).
 33. Marturano, A., Aiello, G., Barra, D., Fedele, L. & Morra, V. Ground movement at Somma-Vesuvius from Last Glacial Maximum. *J. Volcanol. Geotherm. Res.* **211–212**, 24–35 (2012).
 34. Santo, A., Santangelo, N., Beneduce, A. & Iovane, F. Pericolosità connessa a processi alluvionali in aree pedemontane: il caso di Castellammare di Stabia in Penisola Sorrentina. *Il Quaternario* **15**, 23–37 (2002).
 35. Cinque, A. & Irollo, G. Il “Vulcano di Pompeii”: nuovi dati geomorfologici e stratigrafici. *Il Quaternario* **17**, 101–116 (2004).
 36. Cioni, R., Santacroce, R. & Sbrana, A. Pyroclastic deposits as a guide for reconstructing the multi-stage evolution of the Somma-Vesuvius Caldera. *Bull. Volcanol.* **60**, 207–222 (1999).
 37. Andronico, D. & Cioni, R. Contrasting styles of Mount Vesuvius activity in the period between the Avellino and Pompeii Plinian eruptions, and some implications for assessment of future hazards. *Bull. Volcanol.* **64**, 372–391 (2002).
 38. Romano, P. et al. Intersection of exogenous, endogenous and anthropogenic factors in the Holocene landscape: a study of the Naples coastline during the last 6000 years. *Quat. Int.* **303**, 107–119 (2013).
 39. Di Donato, V. et al. Development and decline of the ancient harbor of Neapolis. *Geoarchaeology* **33**, 1–16 (2018).
 40. Keenan-Jones, D. Somma-Vesuvian ground movements and the water supply of Pompeii and the bay of Naples. *Am. J. Archaeol.* **119**, 191–215 (2015).
 41. Roche, O. & Druitt, T. H. Onset of caldera collapse during ignimbrite eruptions. *Earth Planet. Sci. Lett.* **191**, 191–202 (2001).
 42. Fialko, Y. A. & Rubin, A. M. Thermodynamics of lateral dike propagation: Implications for crustal accretion at slow spreading mid-ocean ridges. *J. Geophys. Res. Solid Earth* **103**, 2501–2514 (1998).
 43. Amoroso, A. & Crescentini, L. Shape and volume change of pressurized ellipsoidal cavities from deformation and seismic data. *J. Geophys. Res.* **114**, B02210 (2009).
 44. Galetto, F., Acocella, V., Hooper, A. & Bagnardi, M. Eruption at basaltic calderas forecast by magma flow rate. *Nat. Geosci.* **15**, 580–584 (2022).
 45. Jellinek, A. M. & DePaolo, D. J. A model for the origin of large silicic magma chambers: precursors of caldera-forming eruptions. *Bull. Volcanol.* **65**, 363–381 (2003).
 46. White, S. M., Crisp, J. A. & Spera, F. J. Long-term volumetric eruption rates and magma budgets. *Geochem. Geophys. Geosyst.* **7**, Q03010 (2006).
 47. Macedonio, G., Giudicepietro, F., D’Auria, L. & Martini, M. Sill intrusion as a source mechanism of unrest at volcanic calderas. *J. Geophys. Res.* **119**, 3986–4000 (2014).
 48. Galetto, F., Acocella, V. & Caricchi, L. Caldera resurgence driven by magma viscosity contrasts. *Nat. Commun.* **8**, 1750 (2017).
 49. Santacroce, R., Bertagnini, A., Civetta, L., Landi, P. & Sbrana, A. Eruptive dynamics and petrogenetic processes in a very shallow magma reservoir: the 1906 eruption of Vesuvius. *J. Petrol.* **34**, 383–425 (1993).
 50. Degruyter, W. & Huber, C. A model for eruption frequency of upper crustal silicic magma chambers. *Earth Planet. Sci. Lett.* **403**, 117–130 (2014).
 51. Manga, M. & Brodsky, E. Seismic triggering of eruptions in the far field: volcanoes and geysers. *Annu. Rev. Earth Planet. Sci.* **34**, 263–291 (2006).
 52. Huber, C., Townsend, M., Degruyter, W. & Bachmann, O. Optimal depth of subvolcanic magma chamber growth controlled by volatiles and crust rheology. *Nat. Geosci.* **12**, 762–768 (2019).
 53. Mangler, M. F., Petrone, C. M. & Prytulak, J. Magma recharge patterns control eruption styles and magnitudes at Popocatepetl volcano (Mexico). *Geology* **50**, 366–370 (2022).
 54. Costa, A. & Martí, J. Stress field control during large caldera-forming eruptions. *Front. Earth Sci.* **4**, 92 (2016).
 55. Townsend, M. & Huber, C. A critical magma chamber size for volcanic eruptions. *Geology* **48**, 431–435 (2020).
 56. Rubin, A. M. Propagation of magma-filled cracks. *Annu. Rev. Earth Planet. Sci.* **23**, 287–336 (1995).
 57. Heap, M. J. & Violay, M. E. The mechanical behaviour and failure modes of volcanic rocks: a review. *Bull. Volcanol.* **83**, 33 (2021).
 58. Gregg, P. M. et al. Stress triggering of the 2005 eruption of Sierra Negra volcano, Galápagos. *Geophys. Res. Lett.* **45**, 13288–13297 (2018).
 59. Liao, Y., Soule, S. A., Jones, M. & Le Mével, H. The mechanical response of a magma chamber with poroviscoelastic crystal mush. *J. Geophys. Res.* **126**, e2020JB019395 (2021).
 60. Cioni, R., Gurioli, L., Sbrana, A. & Vougioukalakis, G. Precursors to the Plinian eruptions of Thera (Late Bronze Age) and Vesuvius (AD 79): data from archaeological areas. *Phys. Chem. Earth A* **25**, 719–724 (2000).
 61. González-García, D. et al. Pre-eruptive conditions and dynamics recorded in banded pumices from the El Abrigo Caldera-Forming Eruption (Tenerife, Canary Islands). *J. Petrol.* **63**, egac009 (2022).
 62. Ostorero, L. et al. Correlated petrology and seismicity indicate rapid magma accumulation prior to eruption of Kizimen volcano Kamchatka. *Commun. Earth Environ.* **3**, 290 (2022).

63. Braccini, G. C. *Dell'Incendio Fattosi nel Vesuvio a XVI di Dicembre MDCXXXI* 104 (Secondino Roncagliolo, 1632).
64. Lynn, K. J. & Helz, R. T. Magma storage and transport timescales for the 1959 Kilauea Iki eruption and implications for diffusion chronometry studies using time-series samples versus tephra deposits. *Bull. Volcanol.* **85**, 3 (2022).
65. Ewart, J. A., Voight, B. & Bjornsson, A. Elastic deformation models of Krafla Volcano, Iceland, for the decade 1975 through 1985. *Bull. Volcanol.* **53**, 436–459 (1991).
66. Delgado, F., Contreras-Arratia, R. & Samsonov, S. Magma buoyancy drives rhyolitic eruptions: a tale from the VEI 5 2008–2009 Chaitén eruption (Chile) from seismological and geodetic data. *Earth Planet. Sci. Lett.* **590**, 117564 (2022).
67. Rosi, M. et al. Defining the pre-eruptive states of active volcanoes for improving eruption forecasting. *Front. Earth Sci.* **10**, 795700 (2022).
68. Greco, F., Bonforte, A. & Carbone, D. A long-term charge/discharge cycle at Mt. Etna volcano revealed through absolute gravity and GPS measurements. *J. Geod.* **96**, 101 (2022).
69. Currenti, G. Numerical evidences enabling to reconcile gravity and height changes in volcanic areas. *Geophys. J. Int.* **197**, 164–173 (2014).
70. Scarpa, R., Tronca, F., Bianco, F. & Del Pezzo, E. High resolution velocity structure beneath Mount Vesuvius from seismic array data. *Geophys. Res. Lett.* **29**, 212040 (2002).
71. Piana Agostinetti, N. & Chiarabba, C. Seismic structure beneath Mt Vesuvius from receiver function analysis and local earthquakes tomography: evidences for location and geometry of the magma chamber. *Geophys. J. Int.* **175**, 1298–1308 (2008).
72. Balcone-Boissard, H. et al. Chlorine as a geobarometer for alkaline magmas: evidence from a systematic study of the eruptions of Mount Somma-Vesuvius. *Sci. Rep.* **6**, 21726 (2016).
73. Civetta, L., Galati, R. & Santacroce, R. Magma mixing and convective compositional layering within the Vesuvius magma chamber. *Bull. Volcanol.* **53**, 287–300 (1991).
74. Carey, S. & Sigurdsson, H. Temporal variations in column height and magma discharge rate during the 79 A.D. eruption of Vesuvius. *Geol. Soc. Am. Bull.* **99**, 303–314 (1987).
75. Cioni, R. et al. Compositional layering and syneruptive mixing of a periodically refilled shallow magma chamber: the AD 79 Plinian eruption of Vesuvius. *J. Petrol.* **36**, 739–776 (1995).
76. Marianelli, P., Métrich, N., Santacroce, R. & Sbrana, A. Mafic magma batches at Vesuvius: a glass inclusion approach to the modalities of feeding stratovolcanoes. *Contrib. Mineral. Petrol.* **120**, 159–169 (1995).
77. Morgan, D. J. et al. Magma chamber recharge at Vesuvius in the century prior to the eruption of A.D. 79. *Geology* **34**, 845–848 (2006).
78. Shea, T., Gurioli, L., Houghton, B. F., Cioni, R. & Cashman, K. V. Transition from stable to collapsing column during the 79AD eruption of Vesuvius: the role of pyroclasts density. *Geology* **39**, 695–698 (2011).
79. Cioni, R. Volatile content and degassing processes in the AD 79 magma chamber at Vesuvius (Italy). *Contrib. Mineral. Petrol.* **140**, 40–54 (2000).
80. Ranalli, G. *Rheology of the Earth* 2nd edn, 432 (Springer, 1995).
81. Head, M., Hickey, J., Gottsmann, J. & Fournier, N. The influence of viscoelastic crustal rheologies on volcanic ground deformation: insights from models of pressure and volume change. *J. Geophys. Res.* **124**, 8127–8146 (2019).
82. Dalla Via, G., Sabadini, R., De Natale, G. & Pingue, F. Lithospheric rheology in southern Italy inferred from postseismic viscoelastic relaxation following the 1980 Irpinia earthquake. *J. Geophys. Res.* **110**, 1–16 (2005).
83. Dragoni, M. & Magnanensi, C. Displacement and stress produced by a pressurized, spherical magma chamber, surrounded by a viscoelastic shell. *Phys. Earth Planet. Inter.* **56**, 316–328 (1989).
84. Newman, A. V., Dixon, T. H., Ofoegbu, G. I. & Dixon, J. E. Geodetic and seismic constraints on recent activity at Long Valley Caldera, California: evidence for viscoelastic rheology. *J. Volcanol. Geotherm. Res.* **105**, 183–206 (2001).
85. Newman, A. V., Dixon, T. H. & Gourmelen, N. A four-dimensional viscoelastic deformation model for Long Valley Caldera, California, between 1995 and 2000. *J. Volcanol. Geotherm. Res.* **150**, 244–269 (2006).
86. Del Negro, C., Currenti, G. & Scandura, D. Temperature-dependent viscoelastic modeling of ground deformation: application to Etna volcano during the 1993–1997 inflation period. *Phys. Earth Planet. Inter.* **172**, 299–309 (2009).
87. Zenodo. Archaeological dataset for the 79 CE Vesuvius eruption uplift. <https://doi.org/10.5281/zenodo.7970464> (2023).

Acknowledgements

This work was supported by the INGV project Pianeta Dinamico—Working Earth (CUP 1466 D53J19000170001—“Fondo finalizzato al rilancio degli investimenti delle 1467 amministrazioni centrali dello Stato e allo sviluppo del Paese”, legge 145/2018)—Task V3 (M.A.D.V.), and with the financial support of Presidenza del Consiglio dei Ministri and Dipartimento della Protezione Civile DPC-INGV project. We really thank Teng Wang and Joe Aslin for the editorial work, and Federico Galetto and two anonymous reviewers for helping improve the quality of the manuscript. We also thank Stefano Caliro and Pierangelo Romano for useful discussions on retrospective gas geochemistry.

Author contributions

D.M.D.: writing and editing, petrological and archaeological data input, data interpretation, coordination; E.T.: writing and editing, data interpretation, modelling implementation; I.A.: writing, petrological data input, data interpretation; H.B.B.: writing, petrological data input; D.B.: archaeological data input; G.A.: archaeological data input; V.A.: archaeological data input; M.A.D.V.: writing, petrological and archaeological data input, coordination, funding acquisition.

Competing interests

The authors declare no competing interests.

Additional information

Supplementary information The online version contains supplementary material available at <https://doi.org/10.1038/s43247-023-00880-9>.

Correspondence and requests for materials should be addressed to Domenico M. Doronzo.

Peer review information *Communications Earth & Environment* thanks Federico Galetto, Diego Lobos and the other, anonymous, reviewer(s) for their contribution to the peer review of this work. Primary Handling Editors: Teng Wang and Joe Aslin.

Reprints and permission information is available at <http://www.nature.com/reprints>

Publisher's note Springer Nature remains neutral with regard to jurisdictional claims in published maps and institutional affiliations.



Open Access This article is licensed under a Creative Commons Attribution 4.0 International License, which permits use, sharing, adaptation, distribution and reproduction in any medium or format, as long as you give appropriate credit to the original author(s) and the source, provide a link to the Creative Commons license, and indicate if changes were made. The images or other third party material in this article are included in the article's Creative Commons license, unless indicated otherwise in a credit line to the material. If material is not included in the article's Creative Commons license and your intended use is not permitted by statutory regulation or exceeds the permitted use, you will need to obtain permission directly from the copyright holder. To view a copy of this license, visit <http://creativecommons.org/licenses/by/4.0/>.

© The Author(s) 2023